Journal Pre-proof

An ultracentrifugation – hollow-fiber flow field-flow fractionation orthogonal approach for the purification and mapping of extracellular vesicle subtypes

Valentina Marassi , Serena Maggio , Michela Battistelli , Vilberto Stocchi , Andrea Zattoni , Pierluigi Reschiglian , Michele Guescini , Barbara Roda

PII: S0021-9673(20)31135-3
DOI: https://doi.org/10.1016/j.chroma.2020.461861
Reference: CHROMA 461861

To appear in: *Journal of Chromatography A*

Received date: 4 October 2020
Revised date: 20 December 2020
Accepted date: 27 December 2020

Please cite this article as: Valentina Marassi , Serena Maggio , Michela Battistelli , Vilberto Stocchi , Andrea Zattoni , Pierluigi Reschiglian , Michele Guescini , Barbara Roda , An ultracentrifugation – hollow-fiber flow field-flow fractionation orthogonal approach for the purification and mapping of extracellular vesicle subtypes, *Journal of Chromatography A* (2020), doi: https://doi.org/10.1016/j.chroma.2020.461861

Highlights

- Isolation and characterization of extracellular vesicles (EVs) still remains an analytical challenge
- Combined approaches are required to overcome limitations of commonly employed ultracentrifugation methods
- Ultracentrifugation provides selection of large and small EVs (LEVs and SEVs), while Density Gradient centrifugation can further select homodense SEV particles
- Hollow-fiber flow field-flow fractionation (HF5) with UV, fluorescence and laser scattering detection provides native separation of vesicle subtypes obtained from both processes
- The combined centrifugation-HF5 approach characterized DNA or protein containing particles, free DNA and potential exomeres

An ultracentrifugation – hollow-fiber flow field-flow fractionation orthogonal approach for the purification and mapping of extracellular vesicle subtypes

Valentina Marassi[1,3]*, *Serena Maggio*[2], *Michela Battistelli*[2], *Vilberto Stocchi*[2], *Andrea Zattoni*[1,3], *Pierluigi Reschiglian*[1,3], *Michele Guescini*[2], *Barbara Roda*[1,3]

[1] *Department of Chemistry G. Ciamician, University of Bologna, Bologna, Italy*
[2] *Department of Biomolecular Sciences, University of Urbino Carlo Bo, Urbino, Italy*
[3] *byFlow srl, Bologna, Italy*
*valentina.marassi2@unibo.it

Highlights

- Isolation and characterization of extracellular vesicles (EVs) still remains an analytical challenge
- Combined approaches are required to overcome limitations of commonly employed ultracentrifugation methods
- Ultracentrifugation provides selection of large and small EVs (LEVs and SEVs), while Density Gradient centrifugation can further select homodense SEV particles
- Hollow-fiber flow field-flow fractionation (HF5) with UV, fluorescence and laser scattering detection provides native separation of vesicle subtypes obtained from both processes
- The combined centrifugation-HF5 approach characterized DNA or protein containing particles, free DNA and potential exomeres

Keywords

- Extracellular Vesicles
- Ultracentrifugation
- Hollow-fiber flow field-flow fractionation
- Multi-angle light scattering
- Size and morphology characterization

Abstract

In the course of their life span, cells release a multitude of different vesicles in the extracellular matrix (EVs), constitutively and/or upon stimulation, carrying signals either inside or on their membrane for intercellular communication. As a natural delivery tool, EVs present many desirable advantages, such as biocompatibility and low toxicity. However, due to the complex biogenesis of EVs and their high heterogeneity in size distribution and composition, the characterization and quantification of EVs and their subpopulations still represents an enticing analytical challenge.

Centrifugation methods allow to obtain different subpopulations in an easy way from cell culture conditioned medium and biological fluids including plasma, amniotic fluid and urine, but they still present some drawbacks and limitations. An unsatisfactory isolation can limit their downstream analysis and lead to wrong conclusions regarding biological activities. Isolation and characterization of biologically relevant nanoparticles like EVs is crucial to investigate specific molecular and signaling patterns and requires new combined approaches.

Our work was focused on HF5 (miniaturized, hollow-fiber flow field-flow fractionation), and its hyphenation to utltracentrifugation techniques, which are the most assessed techniques for vesicle isolation. We exploited model samples obtained from culture medium of murine myoblasts (C2C12), known to release different subsets of membrane-derived vesicles.

Large and small EVs (LEVs and SEVs) were isolated by differential ultracentrifugation (UC). Through an HF5 method employing UV, fluorescence and multi-angle laser scattering as detectors, we characterized these subpopulations in terms of size, abundance and DNA/protein content; moreover, we showed that microvesicles tend to hyper-aggregate and partially release nucleic matter. The quali-quantitative information we obtained from the fractographic profiles was improved with respect to Nano Tracking Analysis (NTA) estimation.

The SEV population was then further separated using density gradient centrifugation (DGC), and four fractions were submitted again to HF5-multidetection. This technique is based on a fully orthogonal principle, since F4 does not separate by density, and provided uncorrelated information for each of the fractions processed. The “second dimension” achieved with HF5 showed good promise in sorting particles with both different size and content, and allowed to identify the presence of fibrilloid nucleic matter. This analytical bidimensional approach proved to be effective for the characterization of highly complex biological samples such as mixtures of EVs and could provide purified fractions for further biological characterization.

1. Introduction

Cells can release different types of particles into the extracellular environment: exosomes, shedding vesicles, microvesicles, microparticles, ectosomes and apoptotic bodies. These terms indicate membrane vesicles released by specific cell types and in specific conditions [1] [2]. This heterogeneous population of secreted vesicles, ranging in diameter from 50 to 1000 nm, has recently been defined as extracellular vesicles (EVs) [3]. Among these, exosomes are well defined membrane vesicles (ranging in size from 40 to 100 nm) that are released by cells upon fusion of multivesicular bodies with the plasma membrane. Unlike the proteins trafficked for degradation to the lysosomal system, secreted exosomes are biologically active entities that are important for a variety of pathways [4] [5]. Apoptotic bodies are small membranous particles of 50–5,000 nm in diameter released during the early phase of programmed cell death, and represent the fragments of dying cells, whereas shedding vesicles (or shedding microvesicles) are large EVs ranging between 50–1,000 nm in diameter budding directly from the plasma membrane [3]. Cell-derived vesicles are spherical structures bound by a lipid bilayer, similar in composition to the cell membrane from which the vesicle was derived. Their content includes a variety of cytoplasmic and membrane elements, which is also a reflection of their cell of origin [6]. EVs can be taken up by recipient cells and modulate the activity of target cells, as demonstrated both *in vitro* [7] and *in vivo* [8, 9]. Biochemical techniques have been successfully used to identify protein, mRNA, miRNA, DNA and lipid contents of EVs [10] [11] [12] [13]. Among these, for example, EVs contain a collection of peripheral membrane proteins such as MHC I and II, integrins, transferrin receptors, tetraspanins and GPCRs [14], which can activate downstream signaling pathways in target cells, triggering, for example, calcium signaling , MAPK activation [15], or Fas signaling [16]. Other reports [17, 18], including our previous works [19], have shown that EVs may convey signalling molecules permitting intercellular regulation of gene expression. Altogether, this evidence demonstrates that EVs represent a previously unidentified mode of intercellular exchange of molecular signals. The field of EVs has expanded with the discovery of different types of EVs and the complexity of vesicle biogenesis, cargo loading, release pathways, targeting mechanisms, and vesicle processing. Considering their capacity to transfer bioactive substances, the potential application of EVs in diagnostics and therapeutics has drawn increasing attention. Recent studies introduced the use of EV-based therapy to combat inflammation, though still in an early stage of development [20]. Additionally, EVs physicochemical properties make them a promising vector for drug transport and release in cancer therapy, though the adequate selection of the cell of origin is crucial [21]. As a natural delivery tool, EVs present many desirable advantages, such as biocompatibility, and low

toxicity. To access clinical use it is essential to obtain the accurate size of the carrier particles as well as their size distribution [22]. However, EVs consist in highly heterogeneous bioactive particle populations with complex size distribution and composition, and their characterization and quantification still represent an important analytical challenge.

Various methods for analysis of exosomes include electron microscopy, fluorescence-based detection and tracking techniques; and in particular for exosomes multi-angle light scattering (MALS), nanoparticle-tracking analysis, and dynamic light scattering (DLS) [23]. Currently the most employed approaches to separate EVs and exosomes are based on differential ultracentrifugation, ultracentrifugation in a density gradient, high-pressure liquid chromatography-gel exclusion chromatography and ultrafiltration, and their combination [20, 24-26]. Although these techniques allow to obtain different subpopulations in a fast and easy way from cell culture conditioned medium and biological fluids including plasma, amniotic fluid and urine, they still present some drawbacks and limitations: lower efficiency with biological fluids and modification of native forms and loss of native activity. In addition, contamination of isolated exosomes with non-exosomal particles including proteins limit their downstream analysis and can lead to wrong conclusions regarding biological activities. New combined approaches are required to sort and characterize exosomes and biologically relevant EVs, and to investigate their specific molecular and signaling patterns. Among size-based separation techniques for high molecular weight analytes, field-flow fractionation (FFF) offers to directly obtain a soft, highly-resolved size separation with minimal sample manipulation. The most established FFF variant is flow field-flow fractionation (F4). Coupled with on-line detection methods including multi-angle light scattering (MALS), absorbance and luminescence spectrophotometry, F4 provides uncorrelated information and is able to offer a multidimensional analytical platform for the analysis of particles of biological origin. A wide range of mobile phase compositions, reflective of samples native conditions, can be employed to understand differences between bioparticle sub-populations in a realistic setting.

In F4 the separation is achieved by an external hydrodynamical field, perpendicular to the longitudinal carrier flow, in an empty capillary channel. In F4 retention is inversely proportional to the hydrodynamic diffusion coefficient of the analyte and, consequently, to its M_r or hydrodynamic size. F4 selectivity is particularly high in the high-M_r and nanometer-size range. F4 coupled on-line with multiple detectors is able to separate and characterize populations such as proteins, colloids, polymers and particulate materials up to about 100 μm in size [27].

F4 was already applied to the the analysis of exosomes from cell lines: the ability to detect consistent and subtle differences within populations together with the study of proteomic and lipidomic profiles of different subpopulations, also as a consequence of an oxidative stress, were in

depth demonstrated [28] [29] [30, 31] [32, 33]. F4 was also proved able to define different mechanisms of vesicles formation and modification in their release due to pathway inhibitors [34].

The use of F4 was also explored fot the separation of EVs from biological samples: urinary exosomes were isolated and characterized in terms of size, amount and lipidomic contents in healthy controls and patients with prostate cancer [35] [36]. Recent works report many advances for F4 applications to the isolation of extracellular vescicles from human plasma. Platelet EVs expressing surface markers with important roles in the detection of pathologies were isolated from human plasma with immunoaffinity chromatographic method and size-fractionated and characterized with F4 coupled to MALS and DLS [37]. The immunochromatography and F4 hyphenation was also developed in an on-line format providing a fast, controlled and accurate size-based subpopulation of EVs from human plasma for further specific analysis [38], including electrokinetic characterization of F4 using capillary electrophoresis with laser-induced fluorescence [39]. The improvement of EVs isolation from human plasma was also demonstrated with F4 and different sample pre-treatments able to reduce important contaminants such as high-abundance lipoproteins [40] [41].

The analysis of circulatng microRNA in serum was also reported: F4 was used for the rapid separation of different microRNA carriers including exosomes and the determination of microRNA distribution profiles in healthy and cancer patient cases [42] [34].

These endeavors all contributed to the in-depth investigation of the effectiveness of F4 for EVs analysis. Indeed, it is also endorsed as a technique to simplify complex EVs mixtures prior to accurate particle-by-particle characterization [43]. In this work, the miniaturized F4, hollow-fiber flow field-flow fractionation (HF5) was applied for the first time to EVs analysis.

This micro-volume variant to AF4 was demonstrated capable to achieve high performance and low dilution at the same time enhancing bioparticles analysis[44] [45] [46] [47] [48] [49, 50]. HF5 shows indeed a comparable performance to F4 with interesting advantages: the reduced channel volume and operation flowrates, the low dilution of fractionated analytes, and the potentially disposable use. HF5 merges the advantages of being a miniaturized techniques with the absence of need for specific optimization for the separation of various nanoparticles, depending on sample properties, such as purity, density, solubility, hydrophobicity, solution conductivity, and particle isoelectric charge. The miniaturization of the separation step contributes to the improvement of EVs analysis to obtain more robust, versatile, and high-performance separation and characterization due to the low cost, low sample volume, and minimal sample manipulation [51].

Our work was developed with the aim of exploring the extent to which different isolation techniques can be coupled in order to obtain well defined separation and precise characterization in term of size and nature of the biological content of EV subpopulations. We worked with samples obtained from culture medium of murine myoblasts (C2C12 cell line) which are of interest given their proven ability to release signaling vesicles and microvesicles, having an important role in the communication processes within skeletal muscles and between skeletal muscles and other organs[12]. Their complex communication pattern is achieved through the release of signal molecules and vesicles carrying proteins and RNA.

HF5 coupled with multi-angle light scattering (MALS), fluorescence and UV detection (HF5-UV-FLD-MALS) was applied to the separation and characterization of vesicles from C2C12 cell line. First, whole medium was concentrated and purified through differential ultracentrifugation to obtain subpopulations of LEVs and and SEVs. These subpopulations were analyzed with HF5-MALS to gain information on particle size and cargo content, level of enrichmement and release of nucleic matter. Then, SEVs were separated with density gradient centrifugation (DGC) into homodense fraction to again be analyzed through HF5-multidetection. The separation principle of DGC (density) is indeed orthogonal to that of HF5 (hydrodynamical radius), and allows to obtain a bidimensional separation when these two techniques are used together. The approach allows to highlight low abundant species (such as fibrilloid, RNA-carrying species) and distinguish classes of different particles with their size and loading distributions. The conformational and spectroscopical study achieved in this work facilitated the mapping of the content of cellular secretions in terms of size, chemical composition (DNA, RNA, proteins) and density, discriminating between similar vesicles which may shuttle a different signal.

2. Materials and methods

2.1 Extracellular vesicle isolation

C2C12 cells were cultured in DMEM containing 10% heat-inactivated FBS. FBS was previously centrifuged overnight at 4 °C and 110,000g using a SW28 rotor in a Beckman ultracentrifuge, the supernatant was carefully removed with a pipette, passed through a 0.22 µm filter and then added to DMEM. Conditioned medium from 5 x 10^7 cells was collected after 24h. EVs were purified by differential centrifugation for 15 min at 1000g to eliminate cell contamination. Supernatants were further centrifuged for 20 min at 12,000g and subsequently for 20 min at 18,000-20,000g to obtain LEVs. The resulting supernatants were filtered through a 0.22 µm filter and then micro-vesicles were pelleted by ultracentrifugation at 110,000g for 70 min. The SEV pellets were washed in 13 ml PBS, pelleted again and resuspended in PBS. An aliquote of SEVs was then further fractionated through density gradient centrifugation. (Figure 1).

2.2 Optiprep density gradient separation

A discontinuous iodixanol gradient was used to float the EVs purified from plasma. Iodixanol 40% (w/v), 20% (w/v), 10% (w/v) and 5% (w/v) solutions were prepared diluting OptiPrep (60% (w/v) aqueous iodixanol (Axis-Shield) with 0.25 M sucrose/10 mM Tris, pH 7.5 and gradient was performed as reported in Tauro et al.[52]. EVs pellet purified from plasma were resuspended in 500 µl of 0.25 M sucrose/10 mM Tris, pH 7.5 and overlaid onto the top of the gradient. Centrifugation was performed at 110,000g overnight at 4°C. Twelve individual 1 mL gradient fractions were collected, diluted with 13 ml of PBS and then centrifuged at 110,000g for 1 h at 4 °C and resuspended in PBS (Figure 1). Fractions were monitored for the expression of exosomal marker TSG101 and the muscular marker α-Sarcoglycan by Western blotting. The density of each fraction was determined by absorbance at 244 nm of 1:10,000 diluted fractions.

2.3 NTA characterization

Briefly, approximately 0.3 ml supernatant was loaded into the sample chamber of an LM10 unit (Nanosight, Malwern, UK) and three videos of either 30 or 60 seconds were recorded of each sample. Data analysis was performed with NTA 2.1 software (Nanosight). In NTA the paths of unlabelled particles (i.e. microvesicles) acting as point scatterers, undergoing Brownian motion in a 0.25-ml chamber through which a 405 nm laser beam is passed, is determined from a video recording with the mean squared displacement determined for each possible particle. The diffusion coefficient and sphere-equivalent hydrodynamic radius are then determined using the Stokes–

Einstein equation, and results are displayed as a particle size distribution. Samples were analysed using the basic control settings, which resulted in shutter speeds of 30, 6 and 1 milliseconds for the 100-, 200- and 400-nm control beads, respectively (with zero camera gain), and for biological samples the shutter speeds were 30 or 15 milliseconds, with camera gains of between 280 and 560. Software settings for analysis were: Detection Threshold: 5–10; Blur: auto; Minimum expected particle size: 50 nm. Data are presented as the average and standard deviation of the three video recordings. NTA is most accurate between particle concentrations in the range $2x10^8$ to $20x10^8$/ml. When samples contained higher numbers of particles, they were diluted before analysis and the relative concentration was then calculated according to the dilution factor. Control 100 and 400 nm beads were supplied by Duke Scientific (Palo Alto, CA).

2.4 Transmission electron microscopy

For transmission electron microscopy analysis, specimen drops were deposited on formvar-carbon-coated 300 mesh grids. They were immediately fixed with 2.5% glutaraldehyde for 1 min and then negatively stained with 2% (wt/vol) Na-phosphotungstate for 1 min. The observations were carried out by means of a Philips CM10 transmission electron microscope at 80 kV

2.5 Western blotting analysis

For SDS-PAGE, samples containing 10-30 µg of protein were mixed with Laemmli sample buffer (1:1 ratio) and loaded onto 10% SDS-PAGE gels. Subsequently, proteins were blotted to a Polyvinylidene difluoride (PVDF) membrane (Thermo). Primary antibodies used were: Alix (1:1000 dilution, clone sc-49268 Santa Cruz), CD-63 and Tsg101 (1:2000 dilution, clone 4A10 Abcam). Primary antibodies were incubated overnight at 4°C, followed by washing and the application of secondary HRP-conjugated antibody (Pierce). Immune complexes were visualized using the Clarity and/or Clarity Max (Bio-Rad).

2.6 HF5-UV-FLD-MALS.

HF5 analyses were performed using an Agilent 1200 HPLC system (Agilent Technologies, Santa Clara, CA, USA) consisting in a degasser, an isocratic pump, with an Agilent 1100 DAD UV/Vis spectrophotometer combined with an Eclipse® DUALTEC separation system (Wyatt Technology Europe, Dernbach, Germany). The HF5 channel (Wyatt Technology Europe) consisted of two sets of ferrules, gaskets and cap nuts used to seal a polymeric hollow fiber inside a plastic cartridge. The scheme of the HF5 cartridge, its assembly and the modes of operation of the Eclipse® DUALTEC system have already been described elsewhere [53]. The HF5 channels used for the experimental

section were standard cartridges containing a 17 cm long fiber available from Microdyn-Nadir (Wiesbaden, Germany). The hollow fiber was a polyethersulfone (PES) fiber, type FUS with the following characteristics: 0.8 mm ID, 1.3 mm OD, and 10 kDa Mw cut-off, corresponding to an average pore diameter of 5 nm. The ChemStation version B.04.02 (Agilent Technologies) and Wyatt Eclipse @ ChemStation version 3.5.02 (Wyatt Technology Europe) plugin were used to handle separation methods. A 18-angle multiangle light scattering detector model DAWN HELEOS (Wyatt Technology Corporation, Santa Barbara, CA, USA) operating at a wavelength of 658nm, was used to measure the radius of particles in solution. ASTRA® software version 6.1.7 (Wyatt Technology Corporation) was used to handle signals from the detectors (MALS and UV) and to compute the sample rg values. An HF5 method is composed of four steps: focus, focus–injection, elution and elution–injection. During focus the mobile phase enters from both inlet and outlet and stabilizes; during focus–injection, the flow settings remain unvaried while the sample is introduced into the channel through the inlet and focalized in a narrow band. Then, in the elution step, the flow of mobile phase enters the channel inlet and part of it comes out transversely (cross-flow, Vx), while the rest (channel flow, Vc) reaches the detectors; lastly, during elution–injection, no cross-flow is applied allowing for any remaining sample inside the channel to be released; also, the flow is redirected in the injection line as well to clean it before the next injection. The flow conditions for the different HF5 analysis are shown in Table 1 and Table 2. Longitudinal flow is indicated as Vc, while cross/focus flow as Vx. A volume of 30 to 80µL was injected for the characterisation of the sample, that had been diluted 1:3 in PBS before injection. Due to the parabolic flow profile of the carrier flow, smaller particles experience higher flow rates (on the average) than larger ones. In this normal fractionation mode, the particle retention is a function of its apparent diffusion coefficient. Hence, the particle retention volume can be related to its diffusion coefficient, and consequently, to its hydrodynamic diameter (Dh) or radius (Rh) using the Stoke's equation [54]. FlFFF theory rigors are described elsewhere [55]. Multi-angle light scattering (MALS) was used to determine colloidal size. It allows for the determination of particle root mean square radius of gyration (Rg) by measuring the net intensity of light scattered by such particles at a range of fixed angles. The particle Rg is determined by the mass distribution within the particle. Knowing the epsilon and dn/dc parameters for the eluting saple, molar mass can be calculated from Rg[56].

Radius of gyration and molar mass distributions determined by FFF-MALS provide information on the scaling behaviours in solution. The scaling exponent ν is defined by the slope in a double logarithmic logMW – logRg plot, and gives information about the conformation of the molecules in solution. It is theoretically defined for spheres $\nu = 0.33$, random-coil $\nu = 0.5–0.6$, and rod-like structures $\nu \sim 1$ [57, 58].

3. Results and discussion

3.1 Separation of large and small EVs

The C2C12 muscle cell line was used as a model for EV secretion to investigate the FFF ability to isolate and characterize sub-populations of EVs. Upon serum deprivation, the C2C12 cells undergoing myogenic differentiation are subjected to deep membrane rearrangements, so that a complex mixture of EVs, comprising exosomes and shedding microvesicles, is released in the extracellular environment. A serial ultracentrifugation protocol was specifically set up to isolate large and small EVs basing on their differential sedimentation properties (See Figure 1, Material and Methods). The 10,000g pellet was combined with the 18,000g pellet to obtain large EVs (LEVs) as these vesicles share similar features (data not showed), while the small EV pellet (SEVs) was obtained at 100,000g. The reliability of our protocol for large and small EV separation was investigated by western blot analysis using antibodies against well-defined EV markers (Figure 2); in detail, we found that LEVs were positive for Calnexin, a marker for endoplasmic reticulum, negative for CD63 and slightly positive for Tsg101. On the contrary SEVs were negative for Calnexin and positive for CD63 and Tsg101 (Figure 2a).

Nanoparticle tracking assay confirmed that in our conditions LEVs showed a very variable size distribution with an average diameter of 170 nm (85 nm radius, Figure 2b top) while SEVs had an hydrodynamic diameter of about 90 nm (Figure 2b, bottom graph). When examined by transmission electron microscopy (TEM) using negative staining, the obtained EVs appeared as closed rounding vesicles delimited by membrane structures. In more detail, the SEV pellet showed vesicles with an outer dense wall and an inner less dense region of approximately 50-85 nm in diameter (Figure 2d), while LEVs presented a larger size than SEVs of about 170-200 nm in diameter and a few of them presented an electron-dense material delimited by well-defined membrane structure (Figure 2c).

These data are in agreement with current literature showing CD63 and Tsg101 specific markers of exosome-like vesicles whilst endoplasmatic reticulum proteins are present in shedding microvesicles.

3.2 FFF-multidetection of LEVs and SEVs

LEVs and SEVs deriving from differential centrifugation were analysed with HF5-UV-FLD-MALS, using isotonic, pH 7.4 phosphate buffer (PBS) as carrier. The fractograms obtained for the separation of LEVs and SEVs particles are shown in Figure 3 a and b, respectively.

Concerning the LEVs fraction, three bands are identified along the separation: one at 11, one at 20 and one at 25 minutes. This fraction's predominant peak correspons to field release: the particles display aggregation and only a small fraction of the sample is stable in suspension.

The radius or gyration (Rg) is also displayed for each band. For LEVs, MALS calculation shows that the population of band 1 is 53 nm, the one of band 2 is 80 nm and the one of band 3 averages 155 nm. When compared to NTA results (Figure 2b, lower), band 2 is the one that matches the characterization, in agreement with it being the main population which then aggregates into band 3.

The values calculated for SEVs are 42 nm for band 1, 78 nm for band 2 and 147 nm for band 3. Again the NTA-calculated diameter prior to FFF separation was 80 nm, agreeing with band 1 which is the most abundant. The comparison of the two techniques and the presence of different species within the same sample show that differential centrifugation provides enrichment rather than purification, and this reflects onto the uncertainty in size distribution of NTA measurements. For what concerns SEVs, it is also possible to observe the change in absorption/fluorescence behavior when shifting from the species eluted at 12 minutes to the following one (Figure 3b). Fluorescence decreases differently from absorption meaning that the protein cargo is different for the two species: the first band can either contain a higher amount of protein matter or contain particles expressing membrane proteins on their surface, where fluorescence is not shielded.

Further characterization of the three bands is possible when the conformation plot of each band is taken into consideration: by evaluating the log MW-log Rg line and the resulting slope (named v value), different values emerge for each species (Table 3).

Generally, a value of 0.33 corresponds to a solid sphere, while higher values indicate a less compact or elongated structure like a random coil (0.5) or a rod (1). A very low value such as those obtained for band 1 (in both fractions) and band 2 (LEVs) suggests these are very compact structure, in agreement with densely arranged aggregated DNA (band 1 LEVs) and folded proteins in a core-shell structure (SEVs). Band 2 of the SEV fraction displays a value typical for solid spheres, while the less dense, elongated structure indicated for both band 3 (0.61 and 0.62 respectively) is in agreement with particles clamping together into aggregates. [59, 60] [61]

Finally, the use of a diode array detector allows to collect the UV spectrum for each band eluted. In Figure 4 the spectra for each band are shown for LEVs (a, b, c) and SEVs (d, e, f). By the 280/260 ratio ($r_{260/280}$) for each spectrum it is possible to have an estimate of the nature of these particles: the ratio is 0.6 for purified proteins and increases with DNA presence and heterocontamination [62].

For what concerns LEVs, band one has a $r_{260/280}$ of 1.40, band 2 of 1.17 and band 3 of 1.21 (Figure 4 a,b,c respectively). Band 1 is hence composed by free, aggregated nucleic matter. This resonates with the aggregation/degradation of particles found in band 3, that could have released their content

by membrane disruption. The second and third band, instead, are similar and display a smooth absorption profile typical of fatty acids, suggesting the presence of a lipidic membrane[63]. This is in line with what already observed also with TEM imaging, where particles presented a defined outer membrane. The high value of this ratio can also be influenced by scattering effects (more intense at lower wavelenghts) which are due to aggregation and can distort the profile.

The content of SEVs fraction is different, and the main band corresponds to a high protein abundance (the ratio is 0.67), in agreement with what stated earlier, while the second and third result in similar ratios (1.08 and 1.14 respectively) suggesting that they are the same species which partially aggregate.

3.3 Density centrifugation of SEV particles

To further characterize EV sub-populations SEVs obtained from differential centrifugation were then fractionated on sucrose density gradients. Separated EVs were analysed for EV-marker positivity and by nanoparticle tracking assay (Figure 5).

The obtained data show that vesicles floating at a density of 1.06-1.09 mg/dl (Fraction 7) measured 80-100 nm in diameter (Figure 5 b, left) and were positive to Alix, another well-established exosomal marker; whereas heavier vesicles (fraction 10: density of 1.1-1.2 mg/dl) appeared less positive to Alix than F7 vesicles and larger (Figure 5 b, right). In both cases though it is possible to observe high polydispersion since homodense fractions are not necessarily the same size. The Alix-positive DGC-obtained fractions (7 to 10) were then submitted to HF5-UV-FLD-MALS.

3.4 HF5-UV-FLD-MALS of SEV DCG fractions

Following method development, an elution step was added to separate an early eluting band. Indeed, DGC provides a different selection than differential centrifugation, and the homodense fractions obtained showed different heterogeneity.

Overall, five species were detected and are shown in Figure 6 (and numbered in panel b) but DCG fraction 8 is the only one displaying all of them. The overlay between absorption at 280 nm and fluorescence (tuned on protein intrinsic fluorescence) allows to visualize the different content fraction by fraction. The relative intensities of these bands are different between absorption and fluorescence. In fact, the 340 emission maximum (upon excitation at 280nm) is typical for proteins; it is noticeable how the two signals do not increase or decrease simultaneously, meaning that

proteins, though present in all species but the first, are differently allocated and arranged in different particles. This is also in agreement with different radius and conformation trends, as will be discussed below.

The first band, which increases with density and is highest in fraction 10, is very sharp and is eluted at very low Rt, immediately following the void peak. Followingly, band 2 is present in DCG fractions 7 and 8, but did not reach higher density points. Band 3 appears at DCG fraction 8 and its retention time shifts through the fractions, indicating that hydrodynamical size also increased with density. This is not true for band 4, the last one to elute before the aggregates peak corresponding to band 5.

Overlaid in the Figure, the gyration radius calculated for each species, accounting also for band 3 time shift, is displayed. The numerical values are shown in Table 4, together with the conformation plot slope (v value) calculated.

Band 1 had a very high gyration radius considering its low retention time: this suggests that the separation dynamics is not in normal mode, but rather lifting effects due to a highly elongated structure (such as a rod) are in place. The plot slope is negative: with a MW increase, the Rg decreases, originating a denser structure which adds mass without expanding. The radius of band 2 increases with density (i.e. going from fraction 7 to 10), while the v factor decreases from an elongated structure to a more coiled one. The opposite trend is observed for band 3, where the radius goes from 88 nm to 68 nm and at the same time the structure -though compact- gets closer to a solid sphere. The hydrodynamic radius of these particles increases with density (given the shift in retention time directly dependent on r_h), hence they are bigger, with an increased proteic content, and spherical.

Again the size and the conformation of particles revert for band 4, confirming that it is a different species carrying a different proteic load. Rg increases with density, leading to bigger particles, which also increase in load given the v value shift towards a compact sphere. Last, the aggregates reflect the trend and increase in Rg, while keeping constant the value due to the agglomeration of more particles together.

The absorption spectrum also correlated with these results. In Figure 7 the UV spectra corresponding to the five species in DCG fraction 8, taken as representative sample, are shown. The first band had a different profile and in particular the absorption maximum is around 250 nm, typical of RNA and aggregated nucleotides. The other four spectra all peak at 280 nm; by the ratio between absorption at 260 and 280 nm it is possible to estimate a predominant proteic content for the retained samples with limited impurities (shown on each graph).

By combining all results together, it is noticeable how the DGC fractions obtained from SEVs, are not exactly a simplification of the original medium exctract, since density is not a defining parameter for a single population, and differential centrifugation cannot provide resolution between species.

However, by combining UC and DGC with HF5 and online detectors, it is possible to obtain a non-correlated separation into different subpopulations, and to observe the different degree of loading according to particle size and conformation. The characterization of LEVs and SEVs obtained from ultracentrifugation can give insight on the content of these two vesicular populations, but most of all the HF5 analysis of DCG fraction highlighted how very different species coexist at the same density/sedimentation points and allowed for orthogonal (2D) characterization.

This 2D mapping showed that a certain subpopulation is not uniform in size, but rather exist as a distribution of emptier-fuller vesicles with varying protein cargo, which can be more or less reactive to exosome markers. Vesicle subpopulations can vary in hydrodynamic size (thus modulating their activity as carrier) and can follow different trends.

More importantly, with this approach we found evidence of a rod-shaped, RNA-carrying population otherwise invisible. Given the highly dense structure, the elongated morphology, and the RNA presence, this band 1 could be attributed to exomeres [32] with a different degree of aggregation, in agreement with the presence of amyloid precursor protein [64].

Further downstream characterization would still be needed after fraction collection to better identify these subpopulations and understand the different information each one can carry.

4. Conclusions

The isolation and the characterization of EVs pose a series of challenges both in the analytical and the biotechnological field. On one side, such samples require the least possible manipulation, in order to preserve their relevant biological activity; on the other, an efficient separation of different EV sub-populations is fundamental for their characterization and understanding. Ultracentrifugation and density gradient centrifugation are well-assessed techniques to sort EV subpopulations, but a combined approach is necessary to fully “explode” the content of cellular secretion. We here proposed an approach based on ultracentrifugation, density gradient centrifugation and HF5-UV-FLD-MALS. HF5 was particularly suited for this study since it works with reduced amounts of samples and could process samples deriving from sequential isolation steps.

Selection of LEVs and SEVs was obtained via ultracentrifugation, and verified through Western blotting. HF5-multidetection gave further insight on the size and content of the two populations: it

allowed us to observe DNA/RNA release from LEVs, detected the protein content of SEVs and provided a truthful size characterization with enhanced results compared to NTA.

Then, density gradient centrifugation was used to obtain homodense SEVs fractions, which were submitted to HF5 separation. This combined approach achieved an in-depth characterization of the different species detected which were four or five for each fraction; absorption and conformation studies showed how each class of vesicles existed along both a size and a loading distribution. We also identified an otherwise-hidden rod-shaped species carrying nucleic content, found predominantly in the most dense SEVs fractions, which could potentially correspond to exomeres. This experimental setup proved extremely useful in unraveling such a complex and varied sample, and will offer a valid starting point to further conduct studies in which native fractionation of purified vesicles is required.

Authors Credit role

Valentina Marassi: conceptualization; methodology; formal analysis; data curation; Roles/Writing - original draft Writing - review & editing

Serena Maggio: methodology; formal analysis; data curation;

Michela Battistelli: methodology; formal analysis; data curation;

Vilberto Stocchi: Funding acquisition; Writing - review & editing

Andrea Zattoni: Resources; Writing - review & editing

Pierluigi Reschiglian: Funding acquisition; Writing - review & editing

Michele Guescini: conceptualization; methodology; data curation; Roles/Writing - original draft;

Barbara Roda: Conceptualization; methodology; data curation; Roles/Writing - original draft; Writing - review & editing

Declaration of interests

The authors declare that they have no known competing financial interests or personal relationships that could have appeared to influence the work reported in this paper.

References

1. Raposo, G. and W. Stoorvogel, *Extracellular vesicles: exosomes, microvesicles, and friends.* J Cell Biol, 2013. **200**(4): p. 373-83.

2. György, B., et al., *Membrane vesicles, current state-of-the-art: emerging role of extracellular vesicles.* Cellular and Molecular Life Sciences, 2011. **68**(16): p. 2667-2688.
3. Kalra, H., et al., *Vesiclepedia: A Compendium for Extracellular Vesicles with Continuous Community Annotation.* PLOS Biology, 2012. **10**(12): p. e1001450.
4. Meldolesi, J., *Exosomes and Ectosomes in Intercellular Communication.* Current Biology, 2018. **28**(8): p. R435-R444.
5. Yáñez-Mó, M., et al., *Biological properties of extracellular vesicles and their physiological functions.* Journal of Extracellular Vesicles, 2015. **4**(1): p. 27066.
6. van Niel, G., G. D'Angelo, and G. Raposo, *Shedding light on the cell biology of extracellular vesicles.* Nature Reviews Molecular Cell Biology, 2018. **19**(4): p. 213-228.
7. Valadi, H., et al., *Exosome-mediated transfer of mRNAs and microRNAs is a novel mechanism of genetic exchange between cells.* Nature Cell Biology, 2007. **9**(6): p. 654-659.
8. Alvarez-Erviti, L., et al., *Delivery of siRNA to the mouse brain by systemic injection of targeted exosomes.* Nature Biotechnology, 2011. **29**(4): p. 341-345.
9. Wiklander, O.P.B., et al., *Extracellular vesicle in vivo biodistribution is determined by cell source, route of administration and targeting.* Journal of Extracellular Vesicles, 2015. **4**(1): p. 26316.
10. Mensà, E., et al., *Small extracellular vesicles deliver miR-21 and miR-217 as pro-senescence effectors to endothelial cells.* Journal of Extracellular Vesicles, 2020. **9**(1): p. 1725285.
11. Kitai, Y., et al., *DNA-Containing Exosomes Derived from Cancer Cells Treated with Topotecan Activate a STING-Dependent Pathway and Reinforce Antitumor Immunity.* The Journal of Immunology, 2017. **198**(4): p. 1649-1659.
12. Guescini, M., et al., *C2C12 myoblasts release micro-vesicles containing mtDNA and proteins involved in signal transduction.* Experimental Cell Research, 2010. **316**(12): p. 1977-1984.
13. Record, M., et al., *Extracellular vesicles: lipids as key components of their biogenesis and functions.* J Lipid Res, 2018. **59**(8): p. 1316-1324.
14. Guescini, M., et al., *Microvesicle and tunneling nanotube mediated intercellular transfer of g-protein coupled receptors in cell cultures.* Experimental Cell Research, 2012. **318**(5): p. 603-613.
15. Wu, W., et al., *Astrocyte-derived exosome-transported microRNA-34c is neuroprotective against cerebral ischemia/reperfusion injury via TLR7 and the NF-κB/MAPK pathways.* Brain Research Bulletin, 2020. **163**: p. 84-94.
16. Luchetti, F., et al., *Fas Signalling Promotes Intercellular Communication in T Cells.* PLOS ONE, 2012. **7**(4): p. e35766.
17. Maas, S.L.N., X.O. Breakefield, and A.M. Weaver, *Extracellular Vesicles: Unique Intercellular Delivery Vehicles.* Trends in cell biology, 2017. **27**(3): p. 172-188.
18. Tetta, C., et al., *Extracellular vesicles as an emerging mechanism of cell-to-cell communication.* Endocrine, 2013. **44**(1): p. 11-19.
19. Guescini, M., et al., *Extracellular Vesicles Released by Oxidatively Injured or Intact C2C12 Myotubes Promote Distinct Responses Converging toward Myogenesis.* International Journal of Molecular Sciences, 2017. **18**(11): p. 2488.
20. Tang, T.-T., et al., *Extracellular vesicle-based Nanotherapeutics: Emerging frontiers in anti-inflammatory therapy.* Theranostics, 2020. **10**(18): p. 8111-8129.
21. Cabeza, L., et al., *Cancer therapy based on extracellular vesicles as drug delivery vehicles.* Journal of Controlled Release, 2020. **327**: p. 296-315.
22. Meng, W., et al., *Prospects and challenges of extracellular vesicle-based drug delivery system: considering cell source.* Drug Delivery, 2020. **27**(1): p. 585-598.
23. Doyle, L.M. and M.Z. Wang, *Overview of Extracellular Vesicles, Their Origin, Composition, Purpose, and Methods for Exosome Isolation and Analysis.* Cells, 2019. **8**(7): p. 727.
24. Momen-Heravi, F., et al., *Current methods for the isolation of extracellular vesicles.* Biol Chem, 2013. **394**(10): p. 1253-62.
25. Konoshenko, M.Y., et al., *Isolation of Extracellular Vesicles: General Methodologies and Latest Trends.* BioMed Research International, 2018. **2018**: p. 8545347.

26. Szatanek, R., et al., *Isolation of extracellular vesicles: Determining the correct approach (Review).* Int J Mol Med, 2015. **36**(1): p. 11-7.
27. Schachermeyer S, Z.W., *Flow Field-Flow Fractionation: Analysis of Biomolecules and Their Complexes*, in *Field-flow fractionation in Biopolymers Analysis*, C.K. Williams KSR, Editor. 2012. p. 127-138.
28. Zhang, H. and D. Lyden, *Asymmetric-flow field-flow fractionation technology for exomere and small extracellular vesicle separation and characterization.* Nat Protoc, 2019. **14**(4): p. 1027-1053.
29. Sitar, S., et al., *Size Characterization and Quantification of Exosomes by Asymmetrical-Flow Field-Flow Fractionation.* Analytical Chemistry, 2015. **87**(18): p. 9225-9233.
30. Petersen, K.E., et al., *A review of exosome separation techniques and characterization of B16-F10 mouse melanoma exosomes with AF4-UV-MALS-DLS-TEM.* Analytical and Bioanalytical Chemistry, 2014. **406**(30): p. 7855-7866.
31. Osteikoetxea, X., et al., *Improved Characterization of EV Preparations Based on Protein to Lipid Ratio and Lipid Properties.* PLOS ONE, 2015. **10**(3): p. e0121184.
32. Zhang, H., et al., *Identification of distinct nanoparticles and subsets of extracellular vesicles by asymmetric flow field-flow fractionation.* Nature Cell Biology, 2018. **20**(3): p. 332-343.
33. Yang, J.S., et al., *Investigation of lipidomic perturbations in oxidatively stressed subcellular organelles and exosomes by asymmetrical flow field-flow fractionation and nanoflow ultrahigh performance liquid chromatography-tandem mass spectrometry.* Anal Chim Acta, 2019. **1073**: p. 79-89.
34. Agarwal, K., et al., *Analysis of Exosome Release as a Cellular Response to MAPK Pathway Inhibition.* Langmuir, 2015. **31**(19): p. 5440-5448.
35. Oeyen, E., et al., *Ultrafiltration and size exclusion chromatography combined with asymmetrical-flow field-flow fractionation for the isolation and characterisation of extracellular vesicles from urine.* Journal of Extracellular Vesicles, 2018. **7**(1): p. 1490143.
36. Yang, J.S., et al., *Size Dependent Lipidomic Analysis of Urinary Exosomes from Patients with Prostate Cancer by Flow Field-Flow Fractionation and Nanoflow Liquid Chromatography-Tandem Mass Spectrometry.* Analytical Chemistry, 2017. **89**(4): p. 2488-2496.
37. Multia, E., et al., *Fast isolation of highly specific population of platelet-derived extracellular vesicles from blood plasma by affinity monolithic column, immobilized with anti-human CD61 antibody.* Analytica Chimica Acta, 2019. **1091**: p. 160-168.
38. Multia, E., et al., *Automated On-Line Isolation and Fractionation System for Nanosized Biomacromolecules from Human Plasma.* Analytical Chemistry, 2020. **92**(19): p. 13058-13065.
39. Morani, M., et al., *Electrokinetic characterization of extracellular vesicles with capillary electrophoresis: A new tool for their identification and quantification.* Analytica Chimica Acta, 2020. **1128**: p. 42-51.
40. Kim, Y.B., et al., *Evaluation of exosome separation from human serum by frit-inlet asymmetrical flow field-flow fractionation and multiangle light scattering.* Analytica Chimica Acta, 2020. **1124**: p. 137-145.
41. Wu, B., et al., *Separation and characterization of extracellular vesicles from human plasma by asymmetrical flow field-flow fractionation.* Analytica Chimica Acta, 2020. **1127**: p. 234-245.
42. Ashby, J., et al., *Distribution Profiling of Circulating MicroRNAs in Serum.* Analytical Chemistry, 2014. **86**(18): p. 9343-9349.
43. Kruglik, S.G., et al., *Raman tweezers microspectroscopy of circa 100 nm extracellular vesicles.* Nanoscale, 2019. **11**(4): p. 1661-1679.
44. Park, I., et al., *Performance of hollow-fiber flow field-flow fractionation in protein separation.* J Sep Sci, 2005. **28**(16): p. 2043-9.
45. Marassi, V., et al., *Hollow fiber flow field-flow fractionation and size-exclusion chromatography with multi-angle light scattering detection: A complementary approach in biopharmaceutical industry.* Journal of Chromatography A, 2014. **1372**: p. 196-203.
46. Tanase, M., et al., *Role of Carbonyl Modifications on Aging-Associated Protein Aggregation.* Scientific Reports, 2016. **6**(1): p. 19311.

47. Zattoni, A., et al., *Hollow-fiber flow field-flow fractionation of whole blood serum.* Journal of Chromatography A, 2008. **1183**(1): p. 135-142.
48. Marassi, V., et al., *A new approach for the separation, characterization and testing of potential prionoid protein aggregates through hollow-fiber flow field-flow fractionation and multi-angle light scattering.* Analytica Chimica Acta, 2019. **1087**: p. 121-130.
49. Fukuda, J., et al., *Separation and quantification of monoclonal-antibody aggregates by hollow-fiber-flow field-flow fractionation.* Anal Bioanal Chem, 2014. **406**(25): p. 6257-64.
50. Ibrahim, T., et al., *Dye-free determination of the focalization position for the hollow fiber flow field flow fractionation (HF5) of proteins.* Anal Bioanal Chem, 2015. **407**(15): p. 4301-4.
51. Salafi, T., K.K. Zeming, and Y. Zhang, *Advancements in microfluidics for nanoparticle separation.* Lab on a Chip, 2017. **17**(1): p. 11-33.
52. Greening, D.W., et al., *A Protocol for Exosome Isolation and Characterization: Evaluation of Ultracentrifugation, Density-Gradient Separation, and Immunoaffinity Capture Methods*, in *Proteomic Profiling: Methods and Protocols*, A. Posch, Editor. 2015, Springer New York: New York, NY. p. 179-209.
53. Reschiglian, P., et al., *On-Line Hollow-Fiber Flow Field-Flow Fractionation-Electrospray Ionization/Time-of-Flight Mass Spectrometry of Intact Proteins.* Analytical Chemistry, 2005. **77**(1): p. 47-56.
54. Baalousha, M., et al., *Size fractionation and characterization of natural colloids by flow-field flow fractionation coupled to multi-angle laser light scattering.* J Chromatogr A, 2006. **1104**(1-2): p. 272-81.
55. Zattoni, A., et al., *Turbidimetric Detection Method in Flow-Assisted Separation of Dispersed Samples.* Analytical Chemistry, 2003. **75**(23): p. 6469-6477.
56. Reschiglian, P., et al., *Hollow-fiber flow field-flow fractionation with multi-angle laser scattering detection for aggregation studies of therapeutic proteins.* Analytical and Bioanalytical Chemistry, 2014. **406**(6): p. 1619-1627.
57. Striegel, A.M., *Stepan Podzimek: Light scattering, size exclusion chromatography and asymmetric flow field flow fractionation. Powerful tools for the characterization of polymers, proteins and nanoparticles.* Analytical and Bioanalytical Chemistry, 2012. **402**(5): p. 1857-1858.
58. Masuelli, M. and D. Renard, *Advances in Physicochemical Properties of Biopolymers (Part 1)*. 2017: Bentham Science Publishers.
59. Smilgies, D.-M. and E. Folta-Stogniew, *Molecular weight-gyration radius relation of globular proteins: a comparison of light scattering, small-angle X-ray scattering and structure-based data.* Journal of applied crystallography, 2015. **48**(Pt 5): p. 1604-1606.
60. Feroz Jameel, S.H., *Formulation and Process Development Strategies for Manufacturing Biopharmaceuticals*.
61. Corporation, W.T.; Available from: https://www.wyatt.com/solutions/properties/conformation-of-macromolecules-and-nanoparticles.html.
62. *Technical Support Bulletin*. Available from: http://www.bio.davidson.edu/projects/gcat/protocols/NanoDrop_tip.pdf.
63. Sahi, A.K., et al., *Optimizing a detection method for estimating polyunsaturated fatty acid in human milk based on colorimetric sensors.* Materials Science for Energy Technologies, 2019. **2**(3): p. 624-628.
64. Zhang, Q., et al., *Transfer of Functional Cargo in Exomeres.* Cell Reports, 2019. **27**(3): p. 940-954.e6.

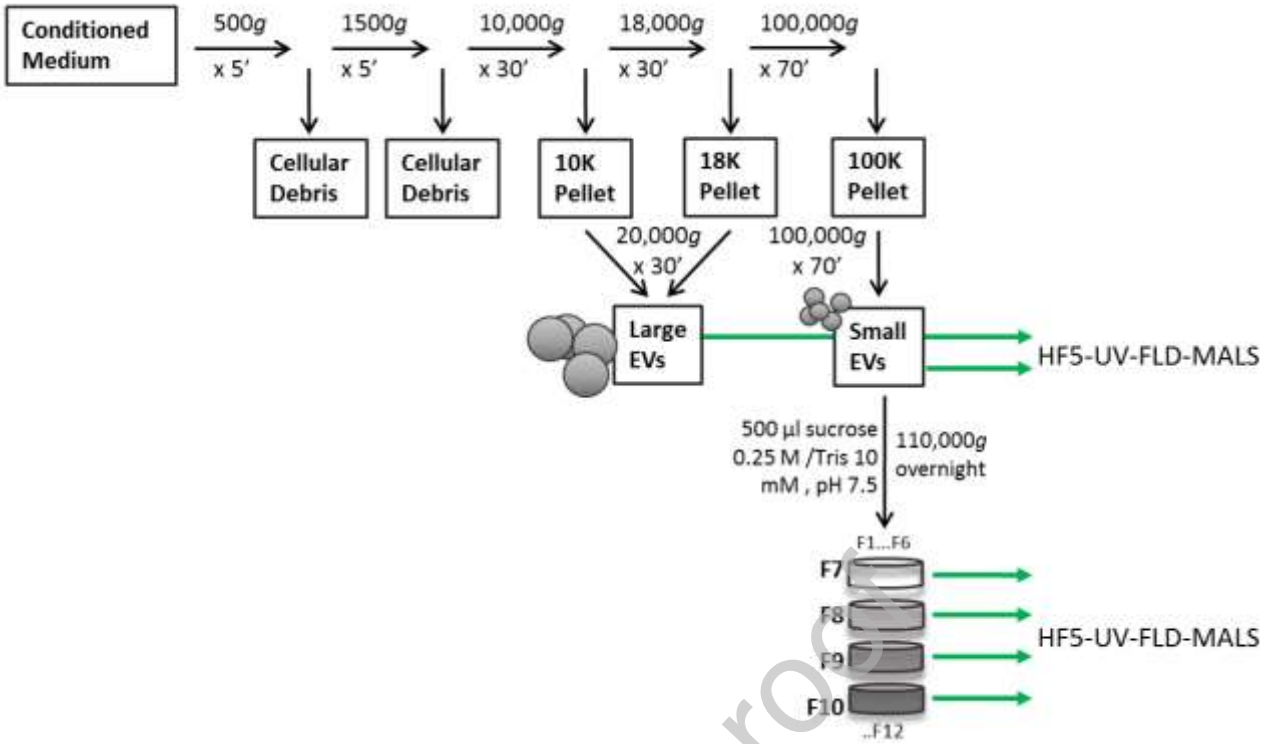

Figure 1. Outline of the overall protocol to produce LEV, SEV and SEV-homodense fractions. Conditioned medium was centrifuged for 5 min at 500g and then for 30 min at 1,500g to remove debris. To pellet LEVs, the supernatant was centrifuged at 10,000g for 30 min and 18,000g for 30 min. The pellets resulting from both centrifuges were joined together and resuspended in PBS followed by ultracentrifugation at 20,000g for 30 min. To collect SEVs, LEV-depleted supernatant was subjected to ultracentrifugation at 100,000g for 70 min. The crude SEV pellet was resuspended in a large volume of PBS followed by ultracentrifugation at 100,000g for 70 min to wash the sample. Last, SEVs were fractionated via Optiprep density gradient centrifugation. They were resuspended in 500 µl of 0.25 M sucrose/10 mM Tris, pH 7.5, overlaid onto the top of the gradient, and centrifuged at 110,000g overnight at 4°C.

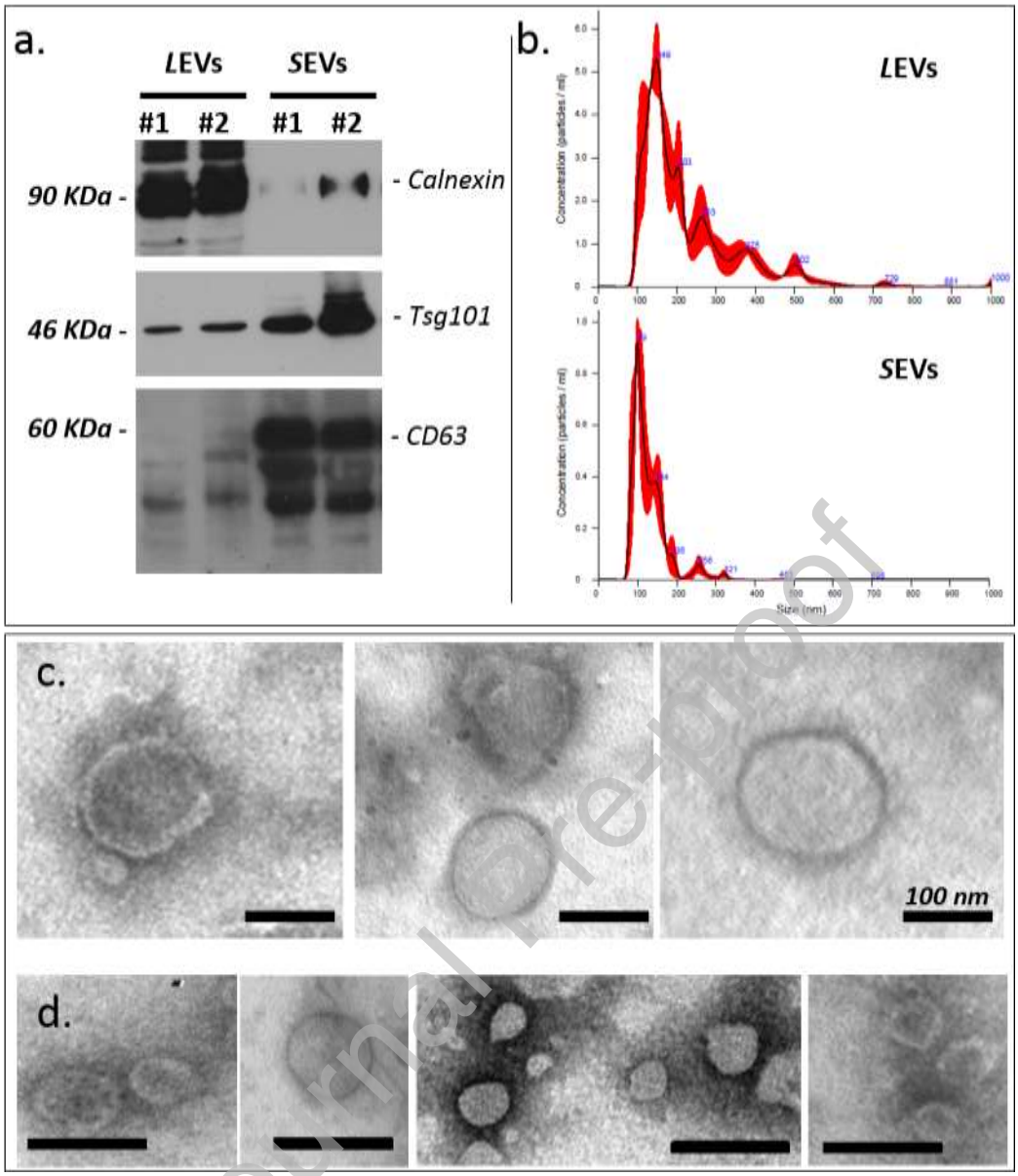

Figure 2. a) Western blot characterization of C2C12 SEVs and LEVs. To pellet LEVs, cell debris-free supernatant was centrifuged at 10,000g for 30 min and 18000g for 30 min. The resulteing pellets were joined and centrifuged at 20,000g for 30 min. To collect SEVs, LEV-depleted supernatant was centrifuged at 100,000g for 70 min. The crude SEV pellet was resuspended in a large volume of PBS followed by ultracentrifugation at 100,000g for 70 min to wash the sample. Blots were probed with antibodies against Tsg101, CD63 (SEVs markers) and Calnexin. Molecular mass markers are shown on the left; b) Nanoparticle tracking assay of the isolated EVs; c,d) TEM analysis of SEVs and LEVS. SEVs (c) appear small vesicles with a diameter of 30- 100 nm and electron-transparent content. LEVs (d) were larger, with a diameter of 100 -400 nm, containing electron-dense material. Scale bar 100nm. Black bars correspond to 100 nm.

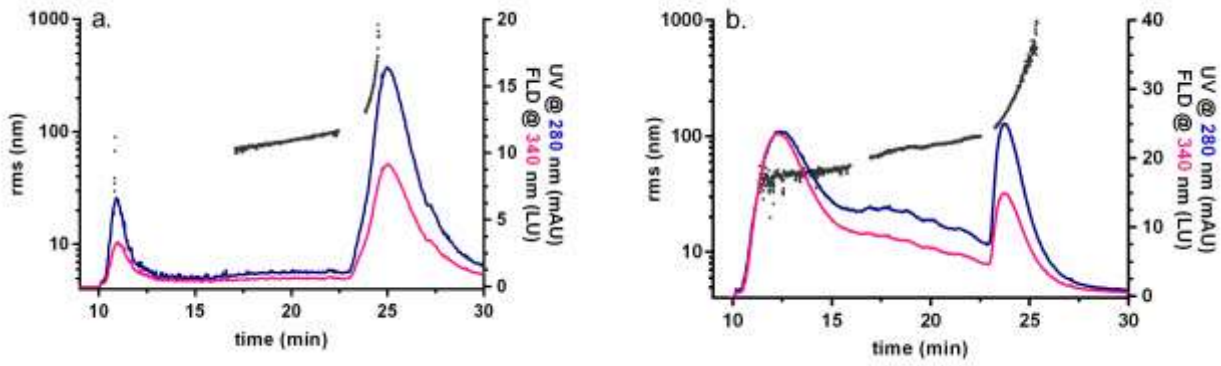

Figure 3. Separation fractograms of LEV (a) and SEV (b) particles. Blue line: UV absorption at 280 nm; pink line: fluorescence emission at 340 nm; Black distribution: radius of gyration calculated from MALS.

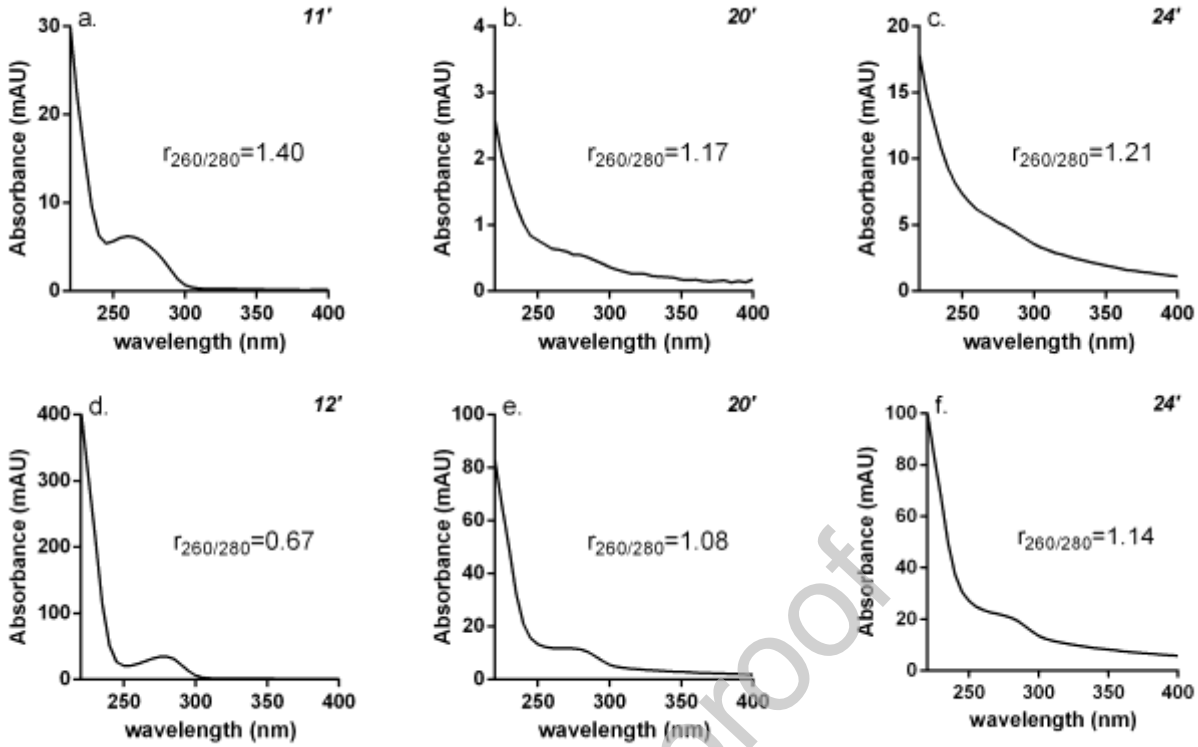

Figure 4. UV spectrum of the three bands of LEV (a, b, c) and SEV (d, e, f) fractions; top right for each panel: timeframe of the extracted spectrum.

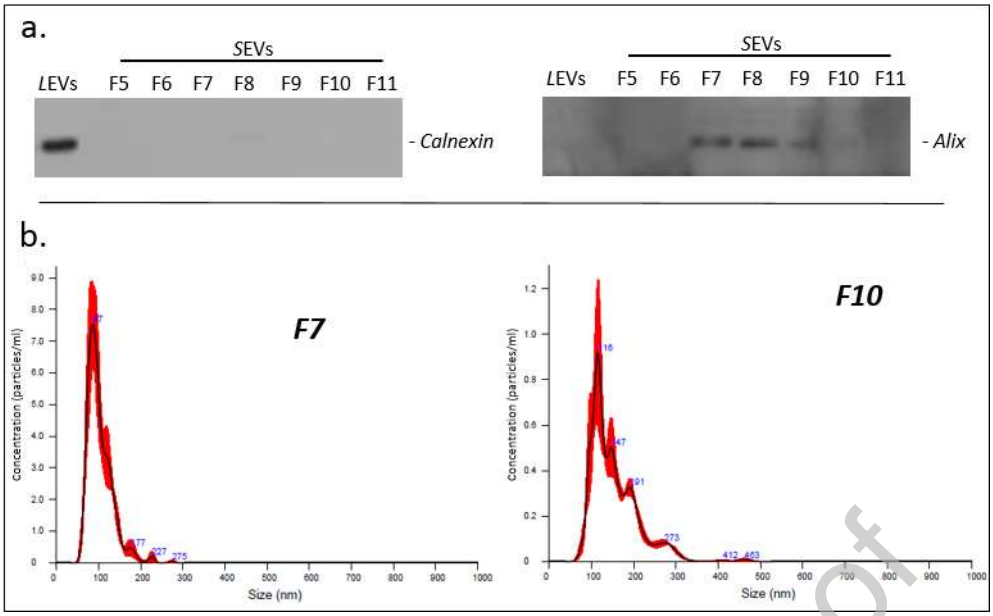

Figure 5. a) SEVs were purified using the serial ultracentrifugation protocol. The obtained pellet was then further separated using the Optiprep iodixanol density gradient. The obtained fractions were identified by Western blot analysis with antibodies against Alix (positive control) and Calnexin (negative control). LEVs were used as negative control.; b) NTA results for SEV Fractions 7 (top) and 10 (bottom)

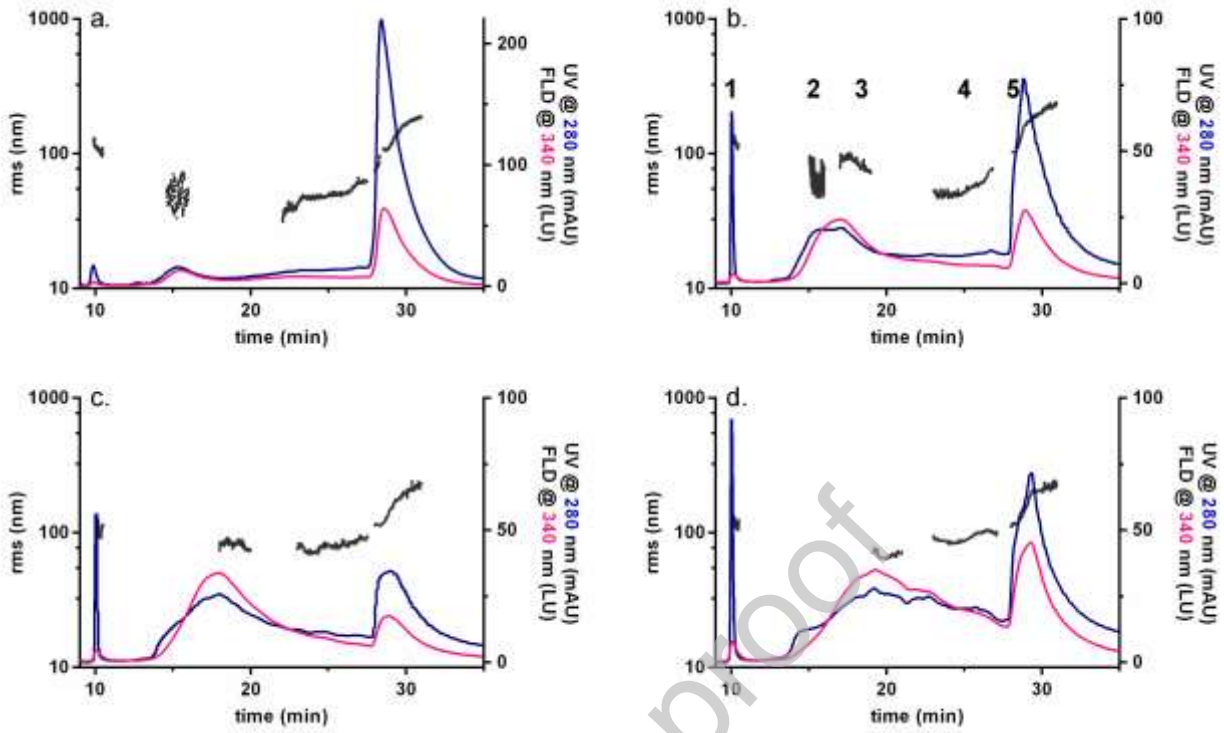

Figure 6. Overlay of UV absorption at 280 nm (blue line), fluorescence emission at 340 nm (pink line) and gyration radius calculated for each species (black distributions) along the FFF separation. a: Fraction 7; b: Fraction 8; c: fraction 9; d: fraction 10.

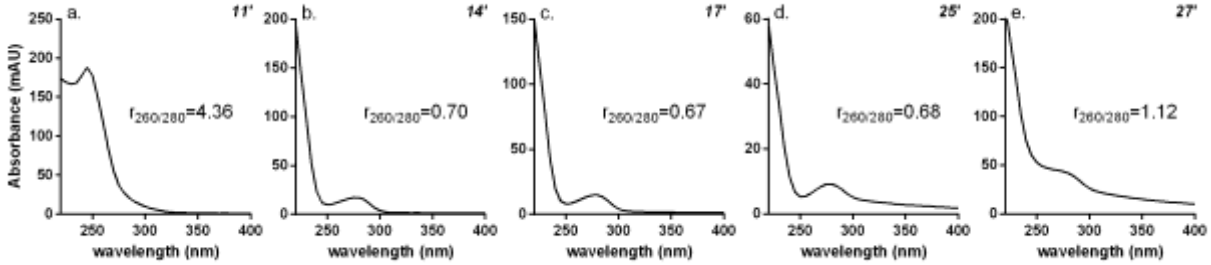

Figure 7. UV spectra of species 1-5 taken from DCG fraction 8 (top right, timepoint of the extracted spectrum). $R_{260/280}$: absorption ratio at the two wavelengths.

Table 1. Flow conditions for HF5 analysis of UC fractions

Steps	Focus (mL/min)	Focus-injection (mL/min)	Elution (mL/min)	Elution (mL/min)	Elution-Inject (mL/min)
Flow rates	Vc=0.35 Vx=0.80 Time=1 min	Vc=0.35 Vx=0.80 Time=8 min	Vc=0.35 Vx=0.05 to 0.03 Time=14 min	Vc=0.35 Vx=0 Time=4 min	Vc=0.35 Vx=0 Time =2 min

Table 2. Flow conditions for HF5 analysis of DGC fractions

Steps	Focus (mL/min)	Focus-injection (mL/min)	Elution (mL/min)	Elution (mL/min)	Elution (mL/min)	Elution-Inject (mL/min)
Flow rates	Vc=0.35 Vx=0.80 Time=1 min	Vc=0.35 Vx=0.80 Time=8 min	Vc=0.35 Vx=0.55 to 0.05 Time=5 min	Vc=0.35 Vx=0.05 to 0.03 Time=14 min	Vc=0.35 Vx=0 Time=4 min	Vc=0.35 Vx=0 Time =2 min

Table 3. v values obtained by the band-specific conformation plots of LEVs and SEVs separation profiles.

Shape factor of species (v value)	**1**	**2**	**3**
LEVs	0.22	0.27	0.61
SEVs	0.14	0.36	0.60

Table 4. Radius and shape factor of each species eluted in the FFF analysis of DCG fractions.

Rg of species (nm)	**1**	**2**	**3**	**4**	**5**
DGC f7	111	50		51	127
DGC f8	132	66	88	57	151
DGC f9	129		82	79	156
DGC f10	145		68	91	165
Shape factor of species (v value)	**1**	**2**	**3**	**4**	**5**
DGC f7	-0.01	0.80		0.61	0.62
DGC f8	-0.12	0.72	0.18	0.59	0.61
DGC f9	-0.15		0.22	0.38	0.63
DGC f10	-0.29		0.32	0.34	0.66